Pairing dynamics in strongly correlated superconductivity

B. Kyung, D. Sénéchal, and A.-M. S. Tremblay
Département de physique and Regroupement québécois sur les matériaux de pointe, Université de Sherbrooke, Sherbrooke, Québec, Canada J1K 2R1
(Received 9 October 2009; published 9 November 2009)

Confirmation of the phononic origin of Cooper pair formation in superconductors came with the demonstration that the interaction was retarded and that the corresponding energy scales were associated with phonons. Using cellular dynamical mean-field theory for the two-dimensional Hubbard model, we identify such retardation effects in *d*-wave pairing and associate the corresponding energy scales with short-range spin fluctuations. We find which frequencies are relevant for pairing as a function of interaction strength and doping and show that the disappearance of superconductivity on the overdoped side coincides with the disappearance of the low-energy feature in the antiferromagnetic fluctuations, as observed in neutron-scattering experiments.

DOI: 10.1103/PhysRevB.80.205109 PACS number(s): 74.20.Mn, 71.10.Fd, 71.30.+h, 74.72.−h

I. INTRODUCTION

In ordinary superconductors, the origin of attraction between electrons, the "pairing glue," manifests itself in observable quantities. Indeed, the characteristic frequencies of phonons appear directly in the frequency dependence of the gap function, which in turn enters observables such as the single-particle density of states (DOS) or the infrared conductivity. Migdal-Eliashberg theory[1,2] has been extremely successful to extract from these experiments the spectral function of the phonons that provide the glue.

High-temperature superconductors, heavy fermions, and layered organic superconductors have phase diagrams, where non-*s*-wave superconducting order parameters lie in close proximity to antiferromagnetic phases. In the case of high-temperature superconductors, much effort has been devoted to find out whether antiferromagnetic fluctuations could be the pairing glue.[3–7] Even though its assumptions are not generally valid in that case, Eliashberg theory has been used to extract the amplitude and frequency dependence of a spectral function that is found to be similar to that for antiferromagnetic fluctuations directly measured by neutron scattering.[8–11]

But understanding the origin of pairing in high-temperature superconductors requires an approach that does *not* rely on the assumptions entering Eliashberg theory and that takes into account Mott insulating behavior. This seems to rule out the theories that are based purely on early weak-coupling ideas of boson exchange.[12–14] In fact, Anderson has argued that the appropriate starting point consistent with Mott physics is the strong-coupling version of the Hubbard model, or the *t*-*J* model. This point of view is challenged, for example, by models involving three bands.[15,16] But even if we focus on the one-band Hubbard model, according to Anderson[17] it is an open issue whether interactions leading to superconductivity are instantaneous,[18] as suggested by resonating valence bond mean-field factorization, or whether they are retarded.[7] In this paper, we show that indeed interactions are retarded and that the corresponding spin fluctuations observed in neutron scattering[19,20] are relevant all the way to the overdoped regime. We also stress the qualitative differences with simple spin-fluctuation ideas.

II. MODEL AND METHOD

We study the Hubbard model Hamiltonian given by

$$H = -\sum_{i,j,\sigma} t_{ij} c^{\dagger}_{i,\sigma} c_{j,\sigma} + U \sum_{i} n_{i\uparrow} n_{i\downarrow}, \tag{1}$$

where t_{ij} and U correspond to the hopping matrix and the on-site screened Coulomb repulsion, respectively, with $c^{(\dagger)}_{i,\sigma}$ being the destruction (creation) operator for an electron at site i with spin σ and $n_{i\sigma}=c^{\dagger}_{i,\sigma}c_{i,\sigma}$ being the number operator. The theoretical method that has been most successful to date to treat the Mott transition starting from the one-band Hubbard model is dynamical mean-field theory (DMFT).[21]

Cluster generalizations of DMFT (Refs. 22–25) are necessary to study problems in two dimensions, where correlations beyond single site must be taken into account to study, for example, *d*-wave superconductivity. They lead to phase diagrams that have the same features as those observed experimentally for both electron-doped and hole-doped high-temperature superconductors[26–29] and for organic conductors. In addition, observable quantities such as the density of states,[28] the angle-resolved photoemission spectroscopy spectrum,[27,28] and the optical conductivity[28] have the experimentally observed behavior. The method that we use, cellular dynamical mean-field theory (CDMFT) with exact diagonalization at $T=0$, is described in Refs. 23 and 27 and in Appendix A and has recently been critically reanalyzed in Ref. 30. It is best to access zero-temperature real-frequency data and to obtain local quantities such as χ'', as we do here. We stress that it does not involve *any* Eliashberg-type approximation.

In CDMFT, antiferromagnetism and *d*-wave superconductivity coexist over part of the phase diagram. This is seen in stoichiometric cuprates with intrinsically doped planes[31] and in a few other cases,[32,33] but does not appear to be a completely generic property of the phase diagram. Our work is thus restricted to showing that spin fluctuations are relevant for high-temperature superconductivity all the way to the overdoped regime, leaving open the possibility that additional types of fluctuations may either contribute to or hinder superconductivity in the underdoped phase.

III. RETARDATION EFFECTS

The correspondence between the imaginary part of the anomalous self-energy, Σ''_{an}, and the imaginary part of the

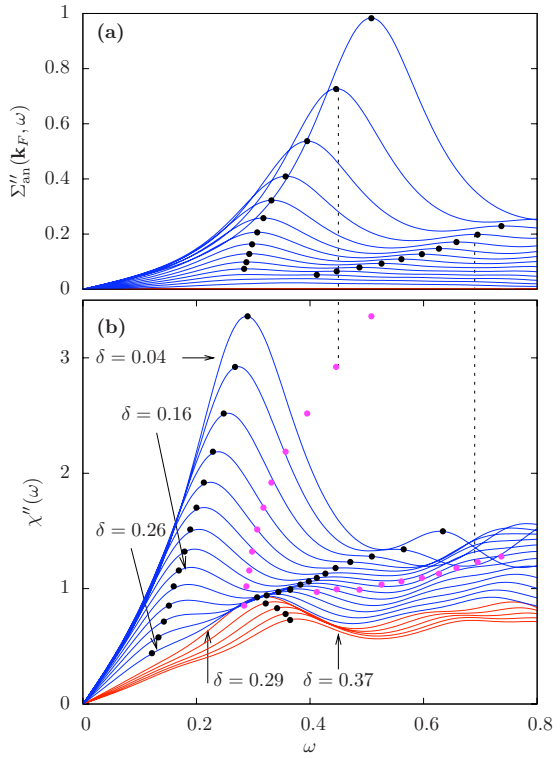

FIG. 1. (Color online) (a) Imaginary part of the anomalous self-energy Im $\Sigma_{an} \equiv \Sigma''_{an}$ at the Fermi wave vector nearest to the antinodal point, for various dopings. (b) Imaginary part of the local spin susceptibility Im $\chi \equiv \chi''$. Black dots in (a) and (b) identify peaks. The position of the peaks of Σ''_{an} in (a) are reported as pale magenta dots in (b) at the same height as the corresponding χ'' to illustrate the correspondence between the main peaks of the two functions. The frequency splitting between the peaks decreases with doping, like the single-particle gap. The red curves are for the normal state. The lower frequency peak present in the superconducting state disappears and the next peak moves to higher frequency with doping. In all the figures, the Lorentzian broadening is $0.125t$, $U=8t$, $t'=-0.3t$, $t''=-0.08t$, for $La_{2-x}Sr_xCuO_4$ and $t=1$, $\hbar=1$.

local spin susceptibility, χ'', is seen in Fig. 1. We take band parameters appropriate for $La_{2-x}Sr_xCuO_4$, namely, $t'=-0.17t$ for nearest-neighbor hopping and $t''=0.08t$ for next-nearest-neighbor hopping. CDMFT with $U=8t$ then leads to superconductivity in the doping range observed experimentally.[27] The anomalous self-energy Σ''_{an} is defined as minus the off-diagonal part of the inverse Green's function in Nambu space. Numerical results are presented in energy units where $t=1$. For all different dopings, the positions of the first two peaks in the spin fluctuations (black dots on bottom panel) (Ref. 28) are just shifted down with respect to the corresponding peaks in Σ''_{an} (black dots on top panel).

In Eliashberg theory for the electron-phonon interactions, the first two peaks in the phonon density of states are shifted down with respect to those in Σ''_{an} by the BCS gap.[7] Similarly, the downshift in peaks in χ'' seen in Fig. 1(b) increases as we underdope, like the single-particle gap. For $U=12t$ and realistic band structure for $YBa_2Cu_3O_{7-x}$ the shift is very weakly doping dependent as seen in Appendix B 2.

In Migdal-Eliashberg theory, the real part of the self-energy Σ'_{an} multiplied by the quasiparticle renormalization factor is the gap function. As discussed further in Appendix B 3, we find that this function has no static contribution, i.e., no frequency-independent contribution at high frequency, contrary to what was found in the t-J model.[7,28] To identify the energy scales relevant for the pairs, we introduce a convenient function, the "cumulative spectral weight of the order parameter"

$$I_F(\omega) \equiv -\int_0^{\omega} \frac{d\omega'}{\pi} \mathrm{Im}\, F^R_{ij}(\omega'). \tag{2}$$

Here F^R is the retarded Gork'ov's function defined in imaginary time by $F_{ij} \equiv -\langle T c_{i\uparrow}(\tau) c_{j\downarrow}(0)\rangle$ with i and j being the nearest neighbors. The infinite frequency limit of $I_F(\omega)$ is equal to $\langle c_{i\uparrow} c_{j\downarrow}\rangle$, which in turn is proportional to the d-wave order parameter (it changes sign under $\pi/2$ rotation). It was shown in Ref. 28 that $\langle c_{i\uparrow} c_{j\downarrow}\rangle$ scales like T_c. For all these reasons, $I_F(\omega)$ is useful to estimate the frequencies relevant for binding. Its meaning is further illustrated by the d-wave BCS result in Fig. 2(a). The function $I_F(\omega)$ rises monotonically until it reaches the sharp BCS cutoff frequency ω_c above which no binding occurs. $I_F(\omega)$ extracted from the Eliashberg calculation[34] for lead is also displayed in Fig. 2(a). The maximum is reached at a frequency just above the largest phonon frequency. Further discussion on $I_F(\omega)$ and

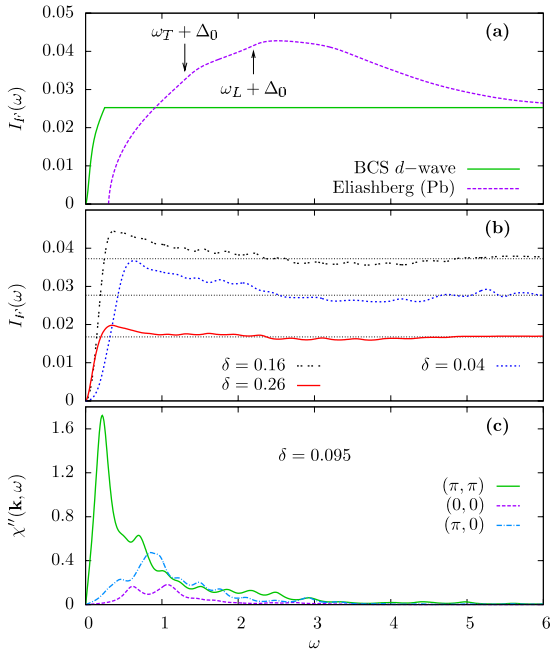

FIG. 2. (Color online) (a) The solid green line is $I_F(\omega)$ for a d-wave BCS superconductor with a cutoff at $\omega_c=0.5$. The dashed magenta line is obtained from Eliashberg theory for Pb in Ref. 34. Frequencies in that case are measured in units of the transverse phonon frequency. The two glitches before the maximum correspond to the transverse and longitudinal peaks in the phonon density of states. The scale of the vertical axis is arbitrary. (b) $I_F(\omega)$ calculated for various dopings. The horizontal lines for the asymptotes mark the value of the order parameter. (c) The three independent Fourier components of χ'' on a 2×2 plaquette for an underdoped case. The (π,π) component dominates at low frequencies. Further examples appear in Appendix C.

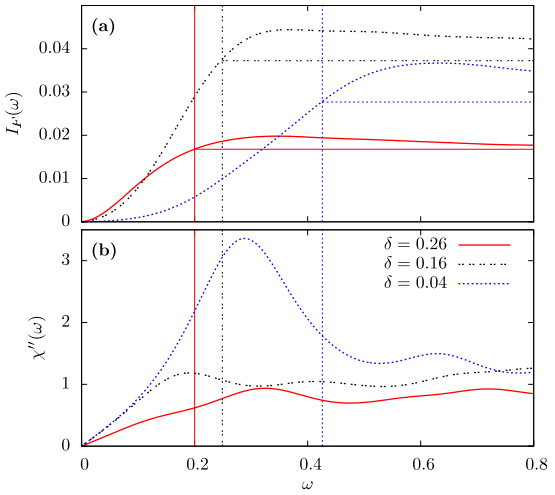

FIG. 3. (Color online) (a) Low-frequency part of $I_F(\omega)$ for three dopings: underdoped, optimally doped, and overdoped. The vertical lines indicate the first intersection with the asymptotic value. The plot of χ'' in (b) shows that the first peak occurs in the frequency interval, where $I_F(\omega)$ reaches its maximum. These are the main frequencies that give rise to pair binding.

calculations in special cases can be found Appendix B 4.

$I_F(\omega)$ is plotted in Fig. 2(b) for underdoping δ=0.04, optimal doping δ=0.16, and overdoping δ=0.26. The asymptotic large frequency value of $I_F(\omega)$ indicated by horizontal lines gives the order parameter that, as a function of doping, has a dome shape dependence.[27] The functions $I_F(\omega)$ cross their respective asymptotic values at progressively lower frequencies as doping increases. The spin fluctuations that dominate at the lower frequencies come from wave vectors around (π,π), as illustrated in Fig. 2(c) for an underdoped case. The maximum of $I_F(\omega)$ is more pronounced in the underdoped regime. The form of $I_F(\omega)$ in the overdoped regime is closer to the BCS limit with just a sharp cutoff. Our calculations are less precise at high frequencies, but nevertheless they suggest that, in all cases, $I_F(\omega)$ undershoots very slightly its asymptotic value and then recovers at frequencies that are of order $U/2$, where the upper Hubbard band opens new scattering channels.[7] This has no analog in ordinary superconductors.

In Fig. 3 we focus on the low-frequency behavior. On the top panel, $I_F(\omega)$ crosses its asymptotic value for the first time near its maximum. This crossing point shown by vertical lines follows the first peak in the corresponding χ'' in the bottom panel. By studying the cases U=8,12,16 we have verified that these features scale with J. Clearly, if we wished to design an approximate mean-field theory[35] for this problem that would play a role analogous to BSC theory as an approximation of the Migdal-Eliashberg theory, we would use a frequency cutoff of order J.

Let us now discuss how the properties of the spin fluctuations $\chi''(\omega)$ correlate with those of the d-wave superconducting state for $La_{2-x}Sr_xCuO_4$. In Fig. 1(b), one sees that in the underdoped regime the low-frequency peak is the most prominent feature. Optimal doping ($\delta \sim 0.16$) is reached when the intensity of the low-frequency peak becomes comparable to the next one at higher frequency. More importantly one sees that, around doping δ=0.26, superconductivity disappears with the low-frequency peak in $\chi''(\omega)$ below ω about $J/2=0.25t$. That low-frequency peak is the one involved in the dynamics of the pairs. To show this, it suffices to check the frequencies in $\chi''(\omega)$ [Fig. 2(b)] that are below the intersection of the $I_F(\omega)$ function with its asymptotic value. Indeed, this intersection is a measure of what would be the cutoff in BCS theory. Note also that the leftover peak in the normal state, indicated in the lowest five curves in Fig. 1(b), moves to higher frequencies as we dope. These features are those found in neutron-scattering experiments[19,20] and are discussed further in Appendix C.

The large tails and monotonic decrease in the weight of the low-frequency peak in χ'' as we dope are consistent with the "glue function" extracted from recent optical conductivity experiments.[11] The position of the low-frequency peak near $0.2t$ at optimal doping is consistent with the experimental value[11] if we take t=250 meV. One should recall that Fig. 1(b), for the local spin spectral weight χ'', gives information integrated in wave vector so the properties of the "neutron resonance" located at (π,π) have to be found by a different approach. In a recent calculation with a related cluster method,[36] it has been found that the peak located at (π,π) in the infinite lattice decreases with frequency in the underdoped regime. Given the small weight of this neutron resonance, this does not contradict the fact that χ'', whether local or averaged over one-quarter of the Brillouin zone (BZ) near (π,π), has the opposite doping dependence.[19,20,37–39] The magnetic resonance itself has small weight.[40]

We stress that, despite the similarities, the results obtained in this paper are not identical to those that are obtained in ordinary superconductors. In particular, in the underdoped regime the spin fluctuations are strongly pair breaking. The pair-breaking effect of the pseudogap can be seen from the fact that in the normal state, the pairing susceptibility decreases as one approaches half-filling when vertex corrections are neglected, as discussed in Appendix B 5. Following the suggestion of Ref. 41, we also checked whether the pseudogap is pair breaking by computing the ratio $\Sigma_{an}(i\omega_n)/(1-\Sigma_n(i\omega_n)/i\omega_n)$ at the antinodal Fermi surface crossing as a function of Matsubara frequency. The ratio is far from constant, in agreement with the existence of strong pair-breaking effects in the pseudogap. From a diagrammatic point of view, spin fluctuations both scatter electrons (self-energy), decreasing the density of states at the Fermi surface, and provide the glue (vertex). This can lead to the dome shape of the transition temperature as a function of doping.[42] In the underdoped regime, the pair-breaking effect wins over the glue provided by the vertex, whereas in the overdoped regime the vertex dominates.

IV. CONCLUSION

We have found that the imaginary part of the anomalous self-energy has a structure that is correlated with the spectrum of local spin fluctuations. This correlation is similar to the one found with the phonon spectrum in the Migdal-Eliashberg theory of ordinary superconductors. This suggests the importance of local spin-one excitations in pair forma-

tion. Our approach also allows for mutual feedback between spin fluctuations and pairing.[43] The frequencies most relevant for the pair dynamics scale with the Heisenberg exchange J. Superconductivity disappears for sufficient overdoping when the first peak in χ'' below frequencies about $J/2$ becomes negligible. There are, however, major differences with simple spin-fluctuation mechanisms. Even though the anomalous self-energy increases as we approach half-filling, the order parameter decreases because of large self-energy effects in the normal part of the propagator. These come from Mott Physics at half-filling. The magnetic fluctuations that we find have the same doping and energy dependence as that found in optical,[9–11] tunneling,[8,44] and neutron experiments.[19,20,37–39] Our work leaves open the possibility that in the underdoped regime there exists other instabilities that compete with antiferromagnetism and d-wave superconductivity. One should also investigate whether retardation is essential to explain why d-wave pairing occurs despite sizable longer range Coulomb repulsion.

ACKNOWLEDGMENTS

We are grateful to D. J. Scalapino for insights at the origin of this work, to W. J. L. Buyers, J. Carbotte, M. Civelli, and T. Maier for discussions, and to M. Greven, G. Kotliar, and L. Taillefer for careful reading and comments on the manuscript. This work was supported by NSERC (Canada), CFI (Canada), the Canadian Institute for Advanced Research, and the Tier I Canada Research chair Program (A.-M.S.T.). Computations were carried out on clusters of the Réseau québécois de calcul de haute performance (RQCHP) and on the Elix cluster at Université de Sherbrooke. A.-M.S.T. thanks the Aspen Center for Physics where this work originated.

APPENDIX A: CELLULAR DYNAMICAL MEAN-FIELD THEORY

In cellular dynamical mean-field theory (CDMFT) a cluster is embedded in a bath of noninteracting electrons that simulates the effect of the rest of the infinite lattice by injecting and removing electrons on the cluster with the appropriate single-particle propagator. The bath is determined self-consistently by requiring that the self-energy of the infinite system and that of the cluster be the same. To break the symmetry, frequency-independent source fields are allowed on bath sites only. More detail can be found in Ref. 27. All the calculations are done with exact diagonalization at zero temperature.[45]

For the case of a 2×2 plaquette, which we shall consider throughout this work, the Nambu spinor is defined by $\Psi_d^\dagger \equiv (c_{1\uparrow}^\dagger,\ldots,c_{4\uparrow}^\dagger,c_{1\downarrow},\ldots,c_{4\downarrow})$, and the Greek letters $\mu,\nu=1,\ldots,N_c$ label the degrees of freedom within the cluster. We compute the cluster propagator $\hat{G}_c$ by solving the cluster impurity Hamiltonian that will be described shortly. Given the $\hat{\mathcal{G}}_0$ on the cluster that results from the presence of the bath, we extract the cluster self-energy from $\hat{\Sigma}_c=\hat{\mathcal{G}}_0^{-1}-\hat{G}_c^{-1}$. Here,

$$\hat{G}_c(\tau,\tau')=\begin{bmatrix}\hat{G}_\uparrow(\tau,\tau') & \hat{F}(\tau,\tau')\\ \hat{F}^\dagger(\tau,\tau') & -\hat{G}_\downarrow(\tau',\tau)\end{bmatrix} \tag{A1}$$

is an 8×8 matrix, $G_{\mu\nu,\sigma}\equiv-\langle Tc_{\mu\sigma}(\tau)c_{\nu\sigma}^\dagger(0)\rangle$ and $F_{\mu\nu}\equiv-\langle Tc_{\mu\uparrow}(\tau)c_{\nu\downarrow}(0)\rangle$ are the imaginary-time-ordered normal and anomalous Green's functions, respectively. Using the self-consistent condition,

$$\hat{\mathcal{G}}_0^{-1}(i\omega_n)=\left[\frac{N_c}{(2\pi)^2}\int d\tilde{\mathbf{k}}\hat{G}(\tilde{\mathbf{k}},i\omega_n)\right]^{-1}+\hat{\Sigma}_c(i\omega_n), \tag{A2}$$

with

$$\hat{G}(\tilde{\mathbf{k}},i\omega_n)=[i\omega_n+\mu-\hat{t}(\tilde{\mathbf{k}})-\hat{\Sigma}_c(i\omega_n)]^{-1}, \tag{A3}$$

we recompute the Weiss field $\hat{\mathcal{G}}_0^{-1}$, obtain the corresponding bath parameters by minimizing a distance function described below, and iterate till convergence. Here $\hat{t}(\tilde{\mathbf{k}})$ is the Fourier transform of the superlattice hopping matrix with appropriate sign flip between propagators for up and down spin and the integral over $\tilde{\mathbf{k}}$ being performed over the reduced Brillouin zone of the superlattice.

A 2×2 plaquette is embedded in a bath of noninteracting electrons. To solve the cluster impurity problem, we express it in the form of a Hamiltonian H_{imp} with a discrete number of bath orbitals coupled to the cluster and use the exact-diagonalization technique (Lanczos method) (Ref. 45)

$$\begin{aligned}H_{\text{imp}}\equiv&\sum_{\mu\nu\sigma}E_{\mu\nu\sigma}c_{\mu\sigma}^\dagger c_{\nu\sigma}+\sum_{m\sigma}\epsilon_{m\sigma}^\alpha a_{m\sigma}^{\dagger\alpha}a_{m\sigma}^\alpha+\sum_{m\mu\sigma}V_{m\mu\sigma}^\alpha(a_{m\sigma}^{\dagger\alpha}c_{\mu\sigma}\\&+\text{h.c.})+U\sum_\mu n_{\mu\uparrow}n_{\mu\downarrow}+\sum_\alpha\Delta^\alpha(a_{1\uparrow}^\alpha a_{2\downarrow}^\alpha-a_{2\uparrow}^\alpha a_{3\downarrow}^\alpha\\&+a_{3\uparrow}^\alpha a_{4\downarrow}^\alpha-a_{4\uparrow}^\alpha a_{1\downarrow}^\alpha+a_{2\uparrow}^\alpha a_{1\downarrow}^\alpha-a_{3\uparrow}^\alpha a_{2\downarrow}^\alpha+a_{4\uparrow}^\alpha a_{3\downarrow}^\alpha-a_{1\uparrow}^\alpha a_{4\downarrow}^\alpha\\&+\text{h.c.}).\end{aligned}$$

Here $\mu,\nu=1,\ldots,N_c$ label the sites in the cluster and $E_{\mu\nu\sigma}$ represents the hopping and the chemical potential within the cluster. The energy levels in the bath are grouped into replicas of the cluster ($N_c=4$) (two replicas in the present case) with the labels $m=1,\cdots,N_c$ and $\alpha=1,2$ such that we have 16 bath energy levels $\epsilon_{m\sigma}^\alpha$ coupled to the cluster via the bath-cluster hybridization matrix $V_{m\mu\sigma}^\alpha$. Using lattice symmetries we take $V_{m\mu\sigma}^\alpha\equiv V^\alpha\delta_{m\mu}$ and $\epsilon_{m\sigma}^\alpha\equiv\epsilon^\alpha$. The quantity Δ^α represents the amplitude of superconducting correlations in the bath. No static mean-field order parameter acts directly on the cluster sites. The parameters ϵ^α, V^α, and Δ^α are determined by imposing the self-consistent condition in Eq. (A2) using a conjugate gradient minimization algorithm with a distance function

$$d=\sum_{\omega_n,\mu,\nu}|[\hat{\mathcal{G}}_0'^{-1}(i\omega_n)-\hat{\mathcal{G}}_0^{-1}(i\omega_n)]_{\mu\nu}|^2 \tag{A4}$$

that emphasizes the lowest frequencies of the Weiss field by imposing a sharp cutoff at $\omega_c=1.5$. (Energies are given in units of hopping t, and we take $\hbar=1$.) The distance function in Eq. (A4) is computed on the imaginary frequency axis (effective inverse temperature, $\beta=50$) since the Weiss field

$\hat{\mathcal{G}}_0(i\omega_n)$ is a smooth function on that axis. With the bond superconducting order parameter defined as

$$\psi_{\mu\nu} = \langle c_{\mu\uparrow} c_{\nu\downarrow} \rangle, \tag{A5}$$

we consider d-wave singlet pairing ($\psi \equiv \psi_{12} = -\psi_{23} = \psi_{34} = -\psi_{41}$). The average is taken in the ground state of the cluster. All quantities depending on the wave vector, including self-energy, are obtained from the Green's function periodization scheme.[46]

The finite size of the bath in the exact-diagonalization technique is an additional approximation to the CDMFT scheme. The accuracy of this approximation can be verified by comparing the CDMFT solution for the one-band Hubbard model with the solution from the Bethe ansatz.[30,47] We have also used this comparison in one dimension as a guideline to fix the choice of parameters in the distance function ($\omega_c = 1.5$ and $\beta = 50$). These results in one dimension also compare well with those obtained using the Hirsch-Fye Quantum Monte Carlo algorithm as an impurity solver where the bath is not truncated.[48] Further, using finite-size scaling for these low (but finite) temperature calculations,[48] it was shown that, at intermediate to strong coupling, a 2×2 cluster in a bath accounts for more than 95% of the correlation effect of the infinite size cluster in the single-particle spectrum. Because of the finite size of the bath, one also needs to use a finite linewidth broadening $\eta = 0.125$ when plotting the figures.

We can also perform an internal consistency check on the effect of the finite bath on the accuracy of the calculation. With an infinite bath, convergence insures that the density inside the cluster is identical to the density computed from the lattice Green's function. In practice, we find that there can be a difference of ± 0.02 between the density estimated from the lattice and that estimated from the cluster. We display results as a function of cluster density since benchmarks with the one-dimensional Hubbard model show that, with a finite bath and the procedure described above, one can reproduce quite accurately Bethe ansatz results for $n(\mu)$ when the cluster density is used. Nevertheless, we should adopt a conservative attitude and keep in mind the error estimate mentioned above.

APPENDIX B: ADDITIONAL INFORMATION ON FIGURES AND FORMULAS

1. Technical comments on Fig. 1

The off-diagonal self-energy Σ''_{an} is extracted from the periodized Nambu Green's function and plotted with $\eta = 0.125$. The maxima of the plot are marked with black dots. The imaginary part of the local spin susceptibility $\chi''(\omega)$ is calculated on the cluster and plotted with the same value of η. The dots indicate the maxima in the limit $\eta = 0$. The various densities evaluated on the cluster are plotted for the following values of (μ, δ) starting from the normal state: (0.25,0.37), (0.375,0.35), (0.5,0.33), (0.625,0.31), (0.75,0.29), (0.875,0.26), (1.0,0.24), (1.125,0.22), (1.25,0.20), (1.375,0.18), (1.5,0.16), (1.625,0.14), (1.75,0.13), (1.875,0.11), (2.0,0.10), (2.125,0.08), (2.25,0.07), (2.375,0.05), and (2.5,0.04).

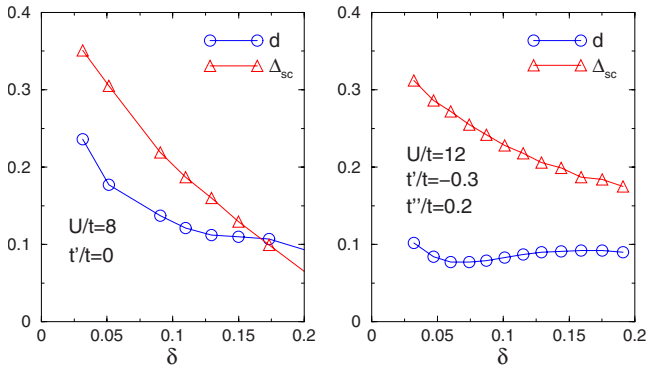

FIG. 4. (Color online) As a function of doping, the shift d (open circles and blue line) between the first peak in the χ'' and the first peak in Σ''_{an} at the antinodal point. Also shown as a function of doping, the single-particle gap Δ_{sc} (triangles and solid red line) measured from the single-particle DOS. On the left panel, $U = 8t$ and $t'/t = 0$. On the right panel $U = 12t$ and the band parameters are those appropriate for $YBa_2Cu_3O_{7-\delta}$.

2. Relation between shift in peak position and single-particle gap

Figure 4 illustrates how the single-particle gap in the superconducting state Δ_{sc} (not necessarily the superconducting gap) and the shift d between the position of the peaks in Σ''_{an} and χ'' change with doping.

3. Real part of the anomalous self-energy

In conventional Migdal-Eliashberg theory, the real part of the self-energy Σ'_{an} multiplied by the quasiparticle renormalization factor is essentially the gap function. We find that this function, illustrated in Fig. 5, increases as one approaches half-filling, consistent with the increase in the single-particle gap found earlier[27] and illustrated in Fig. 4. Σ'_{an} has weak frequency dependence near zero frequency only over a range of order $J = 4t^2/U$ for $U \gtrsim 8t$, as can be seen in Fig. 6. If there were a "static" piece to the gap, Σ'_{an} would have a frequency-

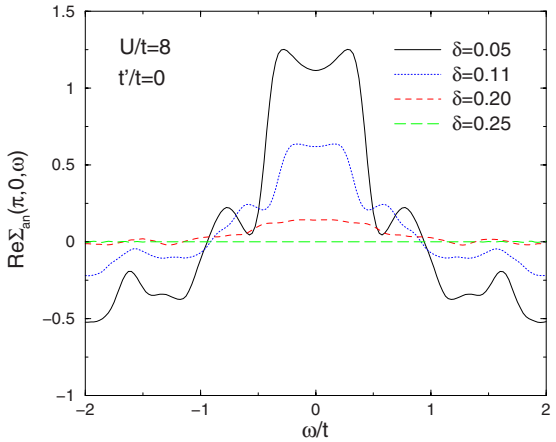

FIG. 5. (Color online) Real part of the anomalous self-energy Σ'_{an} for $U = 8$, $t' = t'' = 0$ at the antinodal point. Four different dopings are presented. Negative contributions appear at a frequency of order J nearly independent of doping.

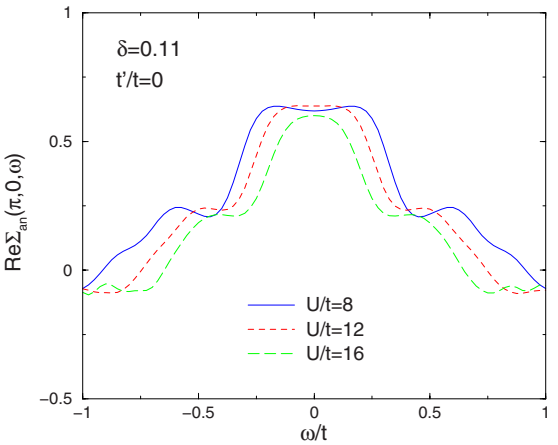

FIG. 6. (Color online) Real part of the anomalous self-energy Σ'_{an} as a function of frequency ω at the antinodal point for fixed doping δ=0.11 and different values of $U=8t, 12t$ and $16t$, $t'=t''=0$ represented, respectively, by solid blue line, short-dashed red line, and long-dashed green line. The nearly flat part near $\omega=0$ decreases with J. The range of frequencies where Σ'_{an} is positive also decreases as U increases or J decreases.

independent component at frequencies larger than J, at least until frequencies of order U. We find that this is not the case. For the t-J model,[7,28] one finds a small instantaneous contribution to Σ'_{an}, thus making connection with mean-field theories. Differences with the t-J model are expected at high frequencies. We show in the main text how mean-field theories can also be seen as approximations to the present approach, even though we do not find an instantaneous contribution to pairing.

4. Cumulative spectral function of the order parameter $I_F(\omega)$

The Lehman representation for the Nambu Green's function allows us to find the following result for the $T=0$ value of $I_F(\omega)$

$$I_F(\omega) = \sum_m \langle 0|c_{i\uparrow}|m\rangle\langle m|c_{j\downarrow}|0\rangle\theta[\omega - (E_m - E_0)], \quad \text{(B1)}$$

with θ being the Heaviside step function. Excited states $|m\rangle$ that contribute have an energy less than ω above the ground state $|0\rangle$.

For BCS s-wave theory, $I_F(\omega)$ can be computed analytically. One obtains, using F^R_{ij} with $i=j$,

$$I_F^{\mathrm{BCS}}(\omega) = \langle c_{i\uparrow}c_{i\downarrow}\rangle\left[\frac{\sinh^{-1}(\omega/\Delta) - \sinh^{-1}(1)}{\sinh^{-1}(\omega_c/\Delta) - \sinh^{-1}(1)} \times \theta(\omega-\Delta)\theta(\omega_c - \omega) + \theta(\omega-\omega_c)\right]. \quad \text{(B2)}$$

The results for the d-wave case in the main text differ from the above. They were obtained by numerical integration and a sharp cutoff. In Eliashberg theory, the function I_F is

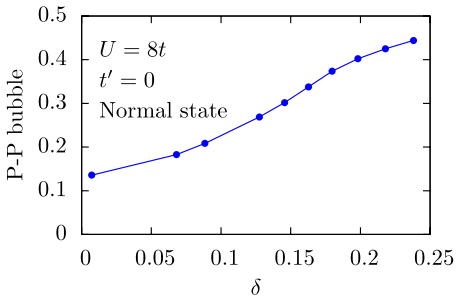

FIG. 7. (Color online) Pairing susceptibility calculated with the dressed bubble only, i.e., without vertex corrections. The decrease near half-filling illustrates the pair-breaking effect of the pseudogap.

$$I_F(\omega) = N(0)\int_0^\omega \mathrm{Re}\left\{\frac{\Sigma_{an}(\omega')}{\sqrt{[Z(\omega')\omega']^2 - \Sigma_{an}(\omega')^2}}\right\}d\omega', \quad \text{(B3)}$$

where $N(0)$ is the single-particle density of states at the Fermi level, the square root is in the upper half-plane and

$$Z(\omega) \equiv 1 - \frac{\Sigma_{11}(\omega) + \Sigma_{22}(\omega)}{2\omega}, \quad \text{(B4)}$$

with $\Sigma_{ii}(\omega)$ being the diagonal components of the self-energy in Nambu space, $\Sigma_{22}(\omega)=-\Sigma_{11}(-\omega)$, and $\Sigma_{an}(\omega)\equiv\Sigma_{12}(\omega)$. The phase is chosen such that there is no contribution from the second Pauli matrix in Nambu space.[34]

The anomalous Green's function $F^R_{ij}(\omega)$ entering the calculation of $I_F(\omega)$ in CDMFT was obtained by Fourier transforming the anomalous lattice Green's function calculated with the band Lanczos approach. We used three different values η=0.24, 0.18, and 0.12 for the small imaginary part that must be added to the real frequency to obtain the retarded $F^R_{ij}(\omega)$. The final result for $I_F(\omega)$ is the extrapolation to $\eta=0$. This is done to smooth the function while preserving as much as possible the asymptotic large frequency value. It differs by only a few percent from the value of the order parameter calculated on the cluster.

5. Effect of the self-energy in decreasing the pairing tendency as one approaches half-filling

Figure 7 shows that in the normal state, the pairing susceptibility calculated without vertex corrections decreases as one approaches half-filling. This is an illustration of the detrimental effect of the pseudogap. The self-energy in the dressed Green's functions entering the calculation leads to a decrease in the number of states that can pair near the Fermi level.

6. Attractive Hubbard model

The cutoff frequency enters very clearly in the integrated off-diagonal spectral weight Eq. (B2). Since one expects that the attractive (instead of repulsive) Hubbard model should behave more like the BCS model, we checked that $I_F(\omega)$ calculated with CDMFT for that model does have the structure of the BCS result for the s wave. In other words, it

vanishes below the gap, and increases monotonically until a sharp cutoff frequency that depends somewhat on U but is on the order of the bandwidth, as expected from the mean-field solution. There is some structure in the frequency dependence that is probably caused in part by the finiteness of the bath used in the calculation, but does not change the overall trend.

APPENDIX C: COMPARISON WITH NEUTRON-SCATTERING EXPERIMENTS

In this Appendix we provide more detail on the comparisons with neutron-scattering experiments. First we recall that we do not focus on the underdoped regime. There may be other complications in the real system as demonstrated by quantum oscillation experiments that suggest Fermi-surface reconstruction. In the underdoped phases, stripes are often present as well. We are asking a question of principle, i.e., what is the mechanism within the one-band Hubbard model, mostly in the overdoped regime. Note also that we are considering the momentum-integrated spin susceptibility, not the one at (π,π). Even within our type of calculations, there are differences between these two cases as we mention in our paper. While the (π,π) spin susceptibility has often been measured, this is not the case for the local spin susceptibility. Figure 8 shows the spin susceptibility at the three independent cluster momenta for two dopings. Even though the (π,π) component is still important at large doping, it does decrease considerably compared with the underdoped case.

The relevant experimental data are for the single-layer material $La_{2-x}Sr_xCuO_4$ (LSCO). We first consider optimal doping on $La_{1.84}Sr_{0.16}CuO_4$ (16% doping), where Fig. 3(a) of Ref. 39 reports the results of neutron scattering for the local spin susceptibility.

In Fig. 1(b) for our numerical results, the curve for doping 0.16 is shown by an arrow. In the experiment, the peaks are located around 20 and 50 meV and are of comparable weight. The two peaks in our results are also of comparable weight and are located around $0.17t$ and $0.30t$. Setting the nearest-neighbor hopping to the typical value $t=250$ meV would lead to theoretical peaks whose energy is about twice too big. Detailed fitting is not the objective of this work. We have checked, however, that increasing U does lead to lower frequency peaks.

Let us now look at the experimental results for the overdoped case, which is the regime that we focus on in our paper. We refer to Fig. 3 of Ref. 20. In this figure, we must disregard the underdoped LBCO results at 1/8 where there are stripes. In the superconducting state of LSCO at 25% doping, the lower energy peak has moved down to energies around 6 meV, i.e., has decreased by a factor of about three in energy compared with optimal doping. In our case, it has decreased by about a factor of two compared with optimal doping. The higher energy peak in the experiment is around 50 meV, i.e., has not moved much compared with optimal doping. This is what happens in our calculation as well. Our calculations show that while there are two main peaks in the superconducting state, when the system becomes normal at 30% doping only the high-energy peak survives and moves to slightly higher energy. This is exhibited clearly in the experimental results of Fig. 3 of Ref. 20.

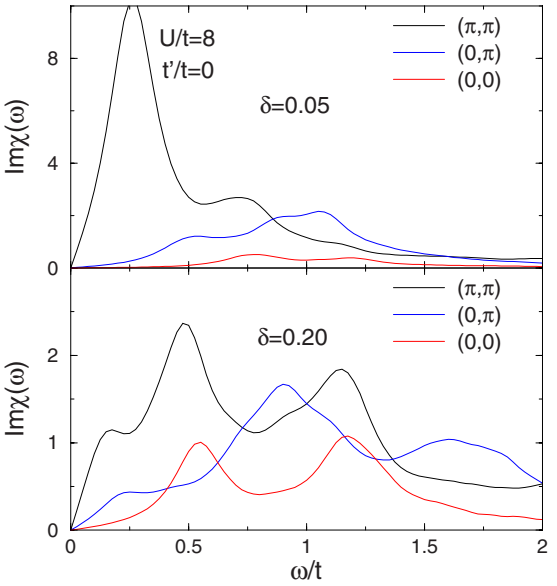

FIG. 8. (Color online) Imaginary part of the spin susceptibility χ'' for $U=8t$, $t'=t''=0$ expressed in cluster momenta for underdoping on the top panel ($\delta=0.05$) and for overdoping on the bottom panel ($\delta=0.2$). Even in the latter case, a sizable (π,π) component is left. We recall that the momenta refer to the averages over a quarter of the BZ.

Experimentally, the intensity of the lowest energy peak in the overdoped regime also decreases with doping. This is shown in Fig. 1 of Ref. 19. The same decrease in intensity is also seen in the numerical results on the first figure of our paper.

The only other experimental results we are aware of for the local spin susceptibility of LSCO are in Fig. 3 of Ref. 49 on $La_{1.915}Sr_{0.085}CuO_4$. The dotted line on this figure allows one to compare the results with those at optimal doping. The high-frequency peak has not moved much but the low-frequency structure has moved down a bit and a new peak has appeared. The new peak and the lowering in frequency differ from our results, but we repeat that other complications such as inhomogeneities may exist in the underdoped regime. We focus on the overdoped case where we showed above that our results mimic the experiments quite closely.

[1] W. L. McMillan and J. M. Rowell, Phys. Rev. Lett. **14**, 108 (1965).
[2] J. P. Carbotte, Rev. Mod. Phys. **62**, 1027 (1990).
[3] N. E. Bickers, D. J. Scalapino, and S. R. White, Phys. Rev. Lett. **62**, 961 (1989).
[4] J. Carbotte, E. Schachinger, and D. Basov, Nature (London) **401**, 354 (1999).
[5] A. V. Chubukov, D. Pines, and J. Schmalian, *The Physics of Superconductors* (Springer-Verlag, Heidelberg, 2003).
[6] P. Monthoux, D. Pines, and G. Lonzarich, Nature (London) **450**, 1177 (2007).
[7] T. A. Maier, D. Poilblanc, and D. J. Scalapino, Phys. Rev. Lett. **100**, 237001 (2008); E. Khatami, A. Macridin, and M. Jarrell, arXiv:0901.4802 (unpublished); M. Civelli, Phys. Rev. Lett. **103**, 136402 (2009).
[8] J. F. Zasadzinski, L. Ozyuzer, L. Coffey, K. E. Gray, D. G. Hinks, and C. Kendziora, Phys. Rev. Lett. **96**, 017004 (2006).
[9] J. Hwang, E. Schachinger, J. P. Carbotte, F. Gao, D. B. Tanner, and T. Timusk, Phys. Rev. Lett. **100**, 137005 (2008).
[10] J. Hwang, J. P. Carbotte, and T. Timusk, Phys. Rev. Lett. **100**, 177005 (2008).
[11] E. van Heumen, E. Muhlethaler, A. B. Kuzmenko, H. Eisaki, W. Meevasana, M. Greven, and D. Van der marel, Phys. Rev. B **79**, 184512 (2009).
[12] M. Beal-Monod, C. Bourbonnais, and V. Emery, Phys. Rev. B **34**, 7716 (1986).
[13] D. J. Scalapino, E. Loh, and J. E. Hirsch, Phys. Rev. B **34**, 8190 (1986).
[14] K. Miyake, S. Schmitt-Rink, and C. M. Varma, Phys. Rev. B **34**, 6554 (1986).
[15] C. M. Varma, Phys. Rev. B **55**, 14554 (1997).
[16] D. C. Peets, D. G. Hawthorn, K. M. Shen, Y.-J. Kim, D. S. Ellis, H. Zhang, S. Komiya, Y. Ando, G. A. Sawatzky, R. Liang, D. A. Bonn, and W. N. Hardy, Phys. Rev. Lett. **103**, 087402 (2009).
[17] P. W. Anderson, Science **316**, 1705 (2007).
[18] G. Kotliar and J. Liu, Phys. Rev. Lett. **61**, 1784 (1988).
[19] S. Wakimoto, H. Zhang, K. Yamada, I. Swainson, H. Kim, and R. J. Birgeneau, Phys. Rev. Lett. **92**, 217004 (2004).
[20] S. Wakimoto, K. Yamada, J. M. Tranquada, C. D. Frost, R. J. Birgeneau, and H. Zhang, Phys. Rev. Lett. **98**, 247003 (2007).
[21] A. Georges, G. Kotliar, W. Krauth, and M. Rozenberg, Rev. Mod. Phys. **68**, 13 (1996).
[22] M. H. Hettler, A. N. Tahvildar-Zadeh, M. Jarrell, T. Pruschke, and H. R. Krishnamurthy, Phys. Rev. B **58**, R7475 (1998).
[23] G. Kotliar, S. Savrasov, G. Pálsson, and G. Biroli, Phys. Rev. Lett. **87**, 186401 (2001).
[24] M. Potthoff, Eur. Phys. J. B **32**, 429 (2003).
[25] T. Maier, M. Jarrell, T. Pruschke, and M. H. Hettler, Rev. Mod. Phys. **77**, 1027 (2005).
[26] D. Sénéchal, P.-L. Lavertu, M.-A. Marois, and A.-M. S. Tremblay, Phys. Rev. Lett. **94**, 156404 (2005).
[27] S. S. Kancharla, B. Kyung, D. Senechal, M. Civelli, M. Capone, G. Kotliar, and A. M. S. Tremblay, Phys. Rev. B **77**, 184516 (2008).
[28] K. Haule and G. Kotliar, Phys. Rev. B **76**, 104509 (2007).
[29] A. Macridin, T. A. Maier, M. S. Jarrell, and G. Sawatzky, Phys. Rev. B **71**, 134527 (2005).
[30] E. Koch, G. Sangiovanni, and O. Gunnarsson, Phys. Rev. B **78**, 115102 (2008).
[31] H. Mukuda, Y. Yamaguchi, S. Shimizu, Y. Kitaoka, P. Shirage, and A. Iyo, J. Phys. Soc. Jpn. **77**, 124706 (2008).
[32] P. Dai, H. J. Kang, H. A. Mook, M. Matsuura, J. W. Lynn, Y. Kurita, S. Komiya, and Y. Ando, Phys. Rev. B **71**, 100502(R) (2005).
[33] J. Chang, A. P. Schnyder, R. Gilardi, H. M. Rønnow, S. Pailhes, N. B. Christensen, Ch. Niedermayer, D. F. McMorrow, A. Hiess, A. Stunault, M. Enderle, B. Lake, O. Sobolev, N. Momono, M. Oda, M. Ido, C. Mudry, and J. Mesot, Phys. Rev. Lett. **98**, 077004 (2007).
[34] D. J. Scalapino, J. R. Schrieffer, and J. W. Wilkins, Phys. Rev. **148**, 263 (1966).
[35] P. W. Anderson, P. A. Lee, M. Randeria, T. M. Rice, N. Trivedi, and F. C. Zhang, J. Phys.: Condens. Matter **16**, R755 (2004).
[36] S. Brehm, E. Arrigoni, M. Aichhorn, and W. Hanke, arXiv:0811.0552 (unpublished).
[37] H. F. Fong, P. Bourges, Y. Sidis, L. P. Regnault, J. Bossy, A. Ivanov, D. L. Milius, I. A. Aksay, and B. Keimer, Phys. Rev. B **61**, 14773 (2000).
[38] O. J. Lipscombe, S. M. Hayden, B. Vignolle, D. F. McMorrow, and T. G. Perring, Phys. Rev. Lett. **99**, 067002 (2007).
[39] B. Vignolle, S. M. Hayden, D. F. McMorrow, H. M. Rønnow, B. Lake, C. D. Frost, and T. G. Perring, Nat. Phys. **3**, 163 (2007).
[40] H.-Y. Kee, S. A. Kivelson, and G. Aeppli, Phys. Rev. Lett. **88**, 257002 (2002).
[41] M. Schiro, M. Capone, M. Fabrizio, and C. Castellani, Phys. Rev. B **77**, 104522 (2008).
[42] B. Kyung, J.-S. Landry, and A. M. S. Tremblay, Phys. Rev. B **68**, 174502 (2003).
[43] C. Bourbonnais and A. Sedeki, Phys. Rev. B **80**, 085105 (2009).
[44] A. N. Pasupathy, A. Pushp, K. K. Gomes, C. V. Parker, J. Wen, Z. Xu, G. Gu, S. Ono, Y. Ando, and A. Yazdani, Science **320**, 196 (2008).
[45] M. Caffarel and W. Krauth, Phys. Rev. Lett. **72**, 1545 (1994).
[46] D. Sénéchal, arXiv:0806.2690 (unpublished).
[47] M. Capone, M. Civelli, S. S. Kancharla, C. Castellani, and G. Kotliar, Phys. Rev. B **69**, 195105 (2004).
[48] B. Kyung, G. Kotliar, and A.-M. S. Tremblay, Phys. Rev. B **73**, 205106 (2006).
[49] O. J. Lipscombe, B. Vignolle, T. G. Perring, C. D. Frost, and S. M. Hayden, Phys. Rev. Lett. **102**, 167002 (2009).